Atmos. Chem. Phys. Discuss., 11, 3071–3115, 2011
www.atmos-chem-phys-discuss.net/11/3071/2011/
doi:10.5194/acpd-11-3071-2011
© Author(s) 2011. CC Attribution 3.0 License.

Atmospheric Chemistry and Physics Discussions

This discussion paper is/has been under review for the journal Atmospheric Chemistry and Physics (ACP). Please refer to the corresponding final paper in ACP if available.

A regional chemical transport modeling to identify the influences of biomass burning during 2006 BASE-ASIA

J. S. Fu[1], N. C. Hsu[2], Y. Gao[1], K. Huang[1], C. Li[2,3], N.-H. Lin[4], and S.-C. Tsay[2]

[1]Department of Civil and Environmental Engineering, University of Tennessee, Knoxville, TN, USA
[2]NASA/Goddard Space Flight Center, Greenbelt, MD, USA
[3]Earth System Science Interdisciplinary Center, University of Maryland, College Park, MD, USA
[4]Department of Atmospheric Sciences, National Central University, Chung-Li, Taiwan

Received: 28 September 2010 – Accepted: 11 January 2011 – Published: 28 January 2011

Correspondence to: J. S. Fu (jsfu@utk.edu)

Published by Copernicus Publications on behalf of the European Geosciences Union.



Abstract

To evaluate the impact of biomass burning from Southeast Asia to East Asia, this study conducted numerical simulations during NASA's 2006 Biomass-burning Aerosols in South-East Asia: Smoke Impact Assessment (BASE-ASIA). Two typical episode periods (27–28 March and 13–14 April) were examined. Two emission inventories, FLAMBE and GFED, were used in the simulations. The influences during two episodes in the source region (Southeast Asia) contributed to CO, O_3 and $PM_{2.5}$ concentrations as high as 400 ppbv, 20 ppbv and 80 μg/m^3, respectively. The perturbations with and without biomass burning of the above three species were in the range of 10 to 60%, 10 to 20% and 30 to 70%, respectively. The impact due to long-range transport could spread over the southeastern parts of East Asia and could reach about 160 to 360 ppbv, 8 to 18 ppbv and 8 to 64 μg/m^3 on CO, O_3 and $PM_{2.5}$, respectively; the percentage impact could reach 20 to 50% on CO, 10 to 30% on O_3, and as high as 70% on $PM_{2.5}$. An impact pattern can be found in April, while the impact becomes slightly broader and goes up to Yangtze River Delta.

Two cross-sections at 15° N and 20° N were used to compare the vertical flux of biomass burning. In the source region (Southeast Asia), CO, O_3 and $PM_{2.5}$ concentrations had a strong upward tendency from surface to high altitudes. The eastward transport becomes strong from 2 to 8 km in the free troposphere. The subsidence contributed 60 to 70%, 20 to 50%, and 80% on CO, O_3 and $PM_{2.5}$, respectively to surface in the downwind area. The study reveals the significant impact of Southeastern Asia biomass burning on the air quality in both local and downwind areas, particularly during biomass burning episodes. This modeling study might provide constraints of lower limit. An additional study is underway for an active biomass burning year to obtain an upper limit and climate effects.

ACPD
11, 3071–3115, 2011



1 Introduction

The aerosols emitted by biomass burning contain a significant fraction of partially oxidized organic carbon and black carbon or soot, which could have significant climatic implications and uncertain (IPCC, 2007). During the combustion process of biomass, substantial amounts of nitrogen oxides, carbon monoxide, and hydrocarbons are produced, which could be precursors of ozone. A positive link between ozone and smoke aerosol has been identified by satellite observation and modeling (Thompson et al., 2001). Aerosol hygroscopic properties could be changed due to the addition of biomass burning aerosol (Kim et al., 2006; Rissler et al., 2006), which further changes cloud microphysical properties (Guyon et al., 2005) and leads to smaller ice crystals and variations of water vapor budget and distribution in the atmosphere (Kim et al., 2009; Sherwood, 2002). The atmospheric temperature profile is also influenced (Davidi et al., 2009), as is solar irradiation due to the aerosol dimming effect (Winkler et al., 2008). Patra et al. (2005) compared the inversion results with biogeochemical model simulations to provide strong evidence that both natural and anthropogenic biomass burning constitute a major component in land-atmosphere carbon flux anomalies. Potter et al. (2001) reported the estimation of carbon losses by biomass burning on the Brazilian Amazonian region from ecosystem modeling and satellite data analysis.

Although biomass burning studies in the last decade have focused on the physical, chemical, and thermodynamic properties of biomass-burning particles (Reid et al., 2005), model simulation results of biomass burning aerosol are still limited. Most of recent model studies focus on Mexico, South America and Africa (Alvarado and Prinn, 2009; Fast et al., 2009; Martins et al., 2009; Milton et al. 2008; Moraes et al., 2004; Myhre et al., 2008; Sinha et al., 2004; Staudt et al. 2002; Trentmann et al., 2002; Zhang et al., 2008), like several recent field projects including SAFARI 2000 (Swap et al., 2003), LAB-SMOCC (Chand et al., 2006; Guyon et al., 2005), the Dust and Biomass-burning Experiment (Haywood et al., 2008) and African Monsoon Multidisciplinary Analysis (Mari et al., 2008).

ACPD
11, 3071–3115, 2011



Southeast Asia is one of the major biomass-burning emission source regions in the world (Streets et al., 2004). Both biomass and fossil combustion processes are potential sources of the extensive Asian Brown Clouds (ABC) over South Asia (Gustafsson et al., 2009). The smoke plume from biomass burning generally spreads downwind thousands of kilometers away and affects air quality, human health, and regional climate. To date, information on the regional distribution of biomass-burning aerosols from Asia remains limited, and their regional radiative impact is not well understood (Wang et al., 2007).

Early studies showed the springtime high ozone events in the lower troposphere from Southeast Asian biomass burning (Liu et al., 1999). The effects of Southeast Asia biomass burning on aerosols and ozone concentrations over the Pearl River Delta (PRD) region was studied using satellite data, ground measurements, and models; it was suggested that O_3 productivity is reduced due to the reduced UV intensity under the influence of Southeast Asia biomass burning (Deng et al., 2008). Choi and Chang (2006) described the use of MOPITT to evaluate the influence of Siberian biomass burning on CO levels around Korea and Japan. Spatial distributions of black carbon (BC) and organic carbon (OC) aerosols were simulated along with the radiative forcing of the Asian biomass burning (Wang et al., 2007). The influence of biomass burning from Southeast Asia on CO, O_3 and radical (OH, HO2) outflow was also simulated by Tang et al. (2003). A new transport mechanism of biomass burning from Indochina was discovered using the WRF/Chem model (Lin et al., 2009). Despite these efforts, however, comprehensive estimates of the impact of Southeast Asia biomass burning on the downstream regions are still lacking.

This study is part of NASA's BASE-ASIA experiment (Biomass-burning Aerosols in South-East Asia: Smoke Impact Assessment; cf. http://smartlabs.gsfc.nasa.gov/) in 2006. One of the objectives of BASE-ASIA is to investigate the regional impact of biomass burning on Southeast and East Asia. This study identifies the influences of biomass burning on East Asia during intense burning episodes by employing a regional "one atmosphere" model, the Community Multiscale Air Quality Modeling

ACPD
11, 3071–3115, 2011



System (CMAQ) (Byun and Schere, 2006; Byun and Ching, 1999). Model simulations were compared with satellite observations and in situ ground measurements to validate the model. Trace gases and particulate matters of biomass burning from model outputs were used to analyze the regional impact of biomass burning on the downstream regions. The goal of this study is to characterize the transport and quantify the impact of biomass burning could from Southeast Asia to East Asia using NASA's 2006 Intercontinental Chemical Transport Experiment-Phase B (INTEX-B) anthropogenic emission inventory (Zhang et al., 2009) and biomass burning emissions (Reid et al., 2009; van der Werf et al., 2006).

2 Methodology

2.1 Model description

This study uses the Models-3/Community Multiscale Air Quality (CMAQ) modeling system. The model has been widely used to predict atmospheric transport in East Asia (Streets, et al., 2007; Carmichael, et al., 2008; Chuang et al., 2008; Fu et al., 2008, 2009a,b; Wang et al, 2008, 2010a,b; Xu et al., 2008). The model configuration is described in Table 1. The modeling domain is shown in Fig. 1.

2.2 Initial profiles of meteorological variables

Meteorological output is considered an important input for CMAQ. The Weather Research and Forecasting (WRF) model, version 3.1.1, was used to achieve meteorological output. To prepare the WRF Preprocessing System (WPS), we used the National Centers for Environmental Prediction (NCEP) Final Analyses dataset (ds083.2) with a resolution of 1.0x1.0 degree grids for every six hours. Objective Analysis (OBSGRID) was performed to adjust the first guess from the WPS output. The input for the OBSGRID includes two parts: observational data, three hourly NCEP Automated Data

ACPD
11, 3071–3115, 2011



Processing (ADP) surface observations (ds464.0), and six hourly upper air and surface observations (ds353.4). The one-way nested approach with four-dimensional data assimilation (FDDA) in WRF was performed from a mother domain with an 81 × 81 km horizontal resolution over Asia nested down to 27 × 27 km. Other WRF configurations are listed in Table 2. A Meteorology/Chemistry Interface Processor (MCIP) 3.4 was used to process the WRF output; the outcome is an input of CMAQ 4.6.

2.3 Emissions

2.3.1 Anthropogenic emissions

Anthropogenic emissions are based on NASA's 2006 Intercontinental Chemical Transport Experiment-Phase B (INTEX-B) emission inventory (Zhang et al., 2009). The inventory mainly includes gaseous pollutants, such as CO_2, SO_2, NO_x, CO, CH_4, and NH_3; non-methane volatile organic compounds (NMVOC); and particulate pollutants, such as submicron black carbon aerosol (BC), submicron organic carbon aerosol (OC), $PM_{2.5}$, and PM_{10}. NMVOC can be categorized into 16 subspecies to match the CB05 mechanism used in CMAQ. The main sources of these emissions are industrial, residential, power plants, and transportation. NH_3 emissions are mainly from six sub-sectors, including cattle, pigs, other animals, fertilizer use, biofuel use, and other sources. The CH_4 emissions were derived from rice cultivation, animal emissions, landfill, wastewater treatment, coal mining/combustion, oil/gas extraction and use, and biofuel combustion (Du, 2008).

2.3.2 Biogenic and biomass burning emissions

Biogenic isoprene emissions were generated from MEGAN to estimate regional and global biogenic emissions. In this study, MEGAN v2.02 was used to generate the hourly biogenic emissions inventories (http://bai.acd.ucar.edu/Megan/index.shtml).

ACPD
11, 3071–3115, 2011



The joint Navy, NASA, NOAA, and universities Fire Locating and Modeling of Burning Emissions (FLAMBE) project was used to investigate a consistent system of emissions (Reid et al., 2009). Hourly emissions from FLAMBE were taken from the 2006 data (http://www.nrlmry.navy.mil/aerosol_web/arctas_flambe/data_hourly/). The fire locations and emissions were computed based on the Global Land Cover Characterization Version 2 database (http://edc2.usgs.gov/glcc/glcc.php). This dataset contains hourly biomass burning areas as well as carbon emissions in a certain location with coordinated latitudes and longitudes.

The Global Fire Emissions Database, Version 2 (GFEDv2.1), another biomass burning emission data source, is derived from MODIS fire count data (van der Werf et al., 2006). This dataset comprises eight-day periods throughout 2006 and monthly average emissions. In this study, carbon emissions from FLAMBE and GFED were both allocated to the simulation domain with a resolution of 27 km × 27 km. Since the temporal resolution of GFED data is eight days, the hourly profile in FLAMBE was used to distribute GFED emissions. Quantitative comparisons between the FLAMBE and GFEDv2.1 biomass emission inventories were conducted in this study before one inventory was selected to further estimate the regional impact of Southeast Asian biomass burning.

Both biomass burning emission inventories estimate carbon emissions, which were then converted to other species. Andreae and Merlet (2001) reported emission factors (EF) for conversion from carbon emissions to other species (CO, CH_4, NMHC, NO_x, NH_3, SO_2, $PM_{2.5}$, TPM, OC and BC) in terms of different land use types, such as tropical forest, extratropical forest, agricultural residues, and savanna and grassland. Based on the 24 land use types (http://www.mmm.ucar.edu/wrf/users/docs/user_guide_V3/users_guide_chap3.htm#_Land_Use_and) and the WRF Preprocessing System (WPS) output, we categorized the land use types into several groups: EF of the grids with land use category 2,3,4 (Dryland Cropland and Pasture, Irrigated Cropland and Pasture, and Mixed Dryland/Irrigated Cropland and Pasture, respectively) were assigned to agricultural residues; EF of the grids with land use category

ACPD
11, 3071–3115, 2011



5,6,7,8,9,10 (Cropland/Grassland Mosaic, Cropland/Woodland Mosaic, Grassland, Shrubland, Mixed Shrubland/Grassland, Savanna, respectively) were assigned to savannas and grasslands; EF of the grids with land use category 11,12,14, 15 (Deciduous Broadleaf Forest, Deciduous Needleleaf Forest, Evergreen Needleleaf, and Mixed Forest, respectively) were assigned to extratropical forests; and the grids with land use category 13 (Evergreen Broadleaf) were assigned to tropical forests. Grids with other land use types usually do not have biomass burnings (van der Werf et al., 2006).

2.3.3 Stratification of biomass burning emission

Determining the inject height is important for the regional chemical model and could significantly affect long-range transport. Leung et al. (2007) used the GEOS-Chem global model to simulate the transport of boreal forest fire smoke under different scenarios and found different CO responses for different injection heights. Freitas et al. (2006) used the 1-D plume rise model to simulate the injection height of fire emissions and found that model outputs were more consistent when the injection height of vigorous fire reached mid-troposphere. Hyer et al. (2007) examined the injection height under five different scenarios using the University of Maryland CTM (Allen et al., 1996a,b) and found that pressure-weighted injection through the tropospheric column into the midtroposphere agreed the best with observations. In this study, we employed SMOKE 2.6, which is widely used to generate emissions for CMAQ, to calculate the inject height of fires based on three parameters, including the bottom height of the plume (Pbot) and the top height of the plume (Ptop). The parameterizations and calculations of Pbot and Ptop are described by Air Sciences, Inc. (2005).

ACPD
11, 3071–3115, 2011



3 In situ and satellite observation

3.1 BASE-ASIA field campaign

During the BASE-ASIA field campaign from February to May 2006, ground-based measurements were conducted at a rural site in Phimai, Thailand. This site was about 260 km to the northeast of Bangkok, about 8 km to the southeast of the local township (population ~10 000), and surrounded by agricultural land. This rural site was rarely influenced by industrial or mobile sources, but occasional local agricultural fires did occur, particularly in March and April. Several trace gases, aerosol optical and microphysical properties, and meteorological parameters were measured with the NASA/GSFC COMMIT (Chemical, Optical, and Microphysical Measurements of In-situ Troposphere) mobile laboratory. The instrumentation of COMMIT has been discussed in detail elsewhere (Li et al., 2010b) and is only briefly introduced here. CO was measured with a modified Thermo Environmental Instruments (Franklin, MA) Model 48C detector (Dickerson and Delany, 1988). A TEI Model 49C was used to monitor O_3. Before and after, as well as every 3–4 weeks during the field campaign, the CO instrument was calibrated with a working standard gas (Scott-Marrin Inc., Riverside, CA) traceable to National Institute of Standards and Technology standard reference materials. The O_3 detector was calibrated with an in-house primary standard (TEI Model 49 PS). Aerosol size distribution was determined with an Aerodynamic Particle Sizer spectrometer (APS, TSI Model 3321) and a Scanning Mobility Particle Sizer (SMPS, TSI Model 3081).

3.2 Other observational sites

The Lulin Atmospheric Background Station (LABS; 23.51° N 120.92° E, 2862 m a.s.l.) is located on the summit of Mt. Front Lulin in Yu-Shan National Park in Central Taiwan. The high-elevation baseline station was established in April 2006 to study the impact of regional and long-range air pollutants on the environment and on ecosystems over

ACPD
11, 3071–3115, 2011



the downwind area of Asia. Continuous operations of precipitation chemistry, aerosol chemistry, trace gases, mercury, atmospheric radiation, and meteorological variables are measured at LABS by various research groups (http://lulin.tw). In this study, CO was measured by HORIBA/APMA-360, with a detection limit of 50 ppb; O_3 was measured by ECOTECH/EC9810, with a detection limit of 0.5 ppb; and PM_{10} was measured by Thermo/R&P 1400a with a detection limit of 0.5 μgm^{-3}. The maximum concentration of pollutants at this site was observed during spring, which corresponds to biomass burning from Southeast Asia (Sheu et al., 2010).

3.3 Satellite observation

A number of satellite sensors launched in the past decade have proven valuable for studying anthropogenic pollution in the troposphere (e.g. Martin, 2008; Richter et al., 2005). In this study, we use the tropospheric NO_2 product from the Ozone Monitoring Instrument (OMI) aboard NASA's EOS Aura satellite, and aerosol optical thickness (AOT) retrieved from the MODerate Resolution Imaging Spectrometer (MODIS) instrument aboard the Aqua satellite (for details of the OMI instrument and NO_2 product, see Levelt et al., 2006 and Bucsela et al., 2006). MODIS provides remotely sensed aerosol information with a resolution of 10 × 10 km for this study. Detailed information on MODIS sensors and global daily observations of aerosols were used to retrieve aerosol properties over land (Kaufman et al., 1997; Hsu et al., 2004, 2006; Levy et al., 2007) and ocean (Tanré et al., 1997). In this study, we use level 2 collection and 5 aerosol optical thickness at 550 nm. Both OMI NO_2 and MODIS AOT products have been widely used in air quality studies to track regional aerosol plumes (Li et al., 2010a) and characterize power plant emissions (Li et al., 2010c).

ACPD
11, 3071–3115, 2011



4 Results and discussion

4.1 Comparison between FLAMBE and GFED emission inventory

We examine biomass burning emissions from five countries in Southeast Asian (Fig. 1): Burma, Laos, Vietnam, Cambodia, and Thailand. The monthly carbon emissions in Southeast Asia derived from FLAMBE and GFEDv2 emission inventories are shown in Table 3, and the monthly carbon emissions from the rest of the model domain (denoted as East Asia) in the two emission inventories are shown in Table 4. Southeast Asia dominated the total carbon emissions in the study domain in both emission inventories, contributing two to three times more biomass burning carbon emissions than East Asia. Moreover, carbon emissions from FLAMBE were 7.58 and 4.86 times that of GFEDv2 for Southeast Asia and East Asia in 2006, respectively (see Tables 3 and 4). The massive divergences between FLAMBE and GFEDv2 (Reid et al., 2009) were mainly due to the difficulty in estimating the emission inventory from the individual fires. The large uncertainty of the method in estimating the carbon emissions can be attributed to higher emission factors for agricultural fires in FLAMBE (Reid et al., 2009).

Although the two emission inventories differed in quantity, they show similar seasonal patterns, with March and April as the most active months in terms of biomass burning. The two months contributed about 70% to the total carbon emissions in GFEDv2. For FLAMBE, the ratio was even higher at about 84%. In spring, the burning of biomass and biofuels was extensive in Southeast Asia; satellite images show that fire spots frequently occurred in the area during this period (Chang and Song, 2010); this was the main cause for the high carbon emissions in these two months. Thus, this period was our main focus for the evaluation of the impact of biomass burning on local and downwind regions. Given the 8- to 12-fold difference between the two inventories for March and April, we drive our models with both and select the inventory that better matches the measurements for further analysis. Here, we choose Phimai, which is located in central Thailand near the biomass burning source regions, to evaluate the model output using the two emission inventories.

ACPD
11, 3071–3115, 2011



Figure 2 shows the comparisons between the observation and simulation results of carbon monoxide (CO), a typical species or tracer for biomass burning sources. The simulation based on FLAMBE emissions agreed well with the surface measurements and successfully captured the peak values from 27 to 28 March and 13 to 14 April. While the simulation based on GFED emissions seemed to model the low CO periods due to relatively weak biomass burning, it obviously underestimated the CO concentrations during the peak periods by as much as 200 to 450 ppbv. This comparison indicates that the FLAMBE emissions provide a better representation of biomass burning sources in our model than the GFED emissions.

Nam et al. (2010) also found underestimation of CO emissions at lower subtropical latitudes over Asia using the GFED emissions. As discussed above, the difference could be attributed to the different methods used to derive the emissions. Additionally, the MODIS satellite observation has limitations in its spatial coverage due to satellite track and clouds; moreover, emissions based on MODIS may not completely cover the study regions at all times. This method also has temporal limitations, as MODIS on board Aqua and Terra could only provide two observations over our study area on a given day.

As stated in Sect. 2.3.2, the GFED emissions were derived from the MODIS eight-day period fire count data; thus, some biomass burning information could be missing, especially for strong episodes. While the FLAMBE emissions provide hourly resolution based on certain assumptions (Reid et al., 2009), the fire emissions estimates are more suitable for this study. Thus, in the further analysis, we use the FLAMBE emissions for sensitivity tests and analysis of the large-scale impact of biomass burning in Southeast Asia.

ACPD
11, 3071–3115, 2011



4.2 Model results and comparison with measurements

4.2.1 Comparison of simulations with site measurements

In this section, we first evaluate the model performance by comparing simulation results with measurement results. Then, we vertically allocate biomass emissions. As described in Sect. 2.3.3, there were two ways to achieve this. One way was to allocate the total biomass burning emissions to the first layer, which was referred to as the SURFACE method, and the other way was to allocate the total biomass burning emissions to different vertical layers, which was referred to as the INJECT method.

Statistical parameters were used for model evaluations. Mean Normalized Bias (MNB) and Mean Normalized Gross Error (MNE) were important parameters to evaluate the model performance; a cutoff of either 40 ppb or 60 ppb for ozone evaluations is recommended by the US EPA (USEPA, 2007). The benchmarks for O_3 MNB and MNE were 15% and 30%, respectively (USEPA, 2007). However, because normalized bias can become large without a threshold (USEPA, 2007), thresholds of 15% and 35% Mean Fractional Bias (MFB) and Mean Fractional Error (MFE) for O_3, and 50% and 75% for $PM_{2.5}$ species were used as recommended by Morris (2005), Morris et al. (2006), and Tesche et al. (2006). The observational datasets at all sites were compared with SURFACE and INJECT model output. The results of model performances for O_3, CO and $PM_{2.5}$ are shown in the Supplement.

Figure S1 shows the results at the source region, Phimai. Most of the parameters, CO, O_3 and $PM_{2.5}$ were within or close to the benchmark according to the USEPA (2007). There was much underestimation for $PM_{2.5}$, which could be related to emissions. As for the four sites in Hong Kong (Fig. S2) and in Lulin (Fig. S3), MFB, MFE, NMB, NME, MNB, MNE of O_3, $PM_{2.5}$ were all within the benchmark, indicating that model performance was reasonable and relatively good. The overestimation of CO could be due to the outflows from inland China or the local biomass emission. When observational concentration was at a relatively low level, O_3 was over-predicted.

ACPD
11, 3071–3115, 2011



Overall, the CMAQ model could simulate reasonably well as suggested by the comparison to various datasets. Moreover, there was not much difference between the two allocation methods. n fact, we still see from the supplemental tables that the INJECT method performed slightly better than the SURFACE method. Based on the Air Sciences, Inc., 2005, we believe that the INJECT methods as a better way to allocate the biomass burning emissions in more layers.

4.2.2 Remote sensing observations

We also evaluate the model performance against remote sensing data during two biomass burning episodes. As shown in Table 3, the largest CO emission rate occurred in March and April. The TRACE-P Project during the same season (Tang et al., 2003) indicated that biomass burning was ubiquitous in Southeast Asia during this period. We found that the peak values did not coincide between days among different years. This is because biomass burning emissions were highly episodic. Due to irregular biomass burning from wildfires or anthropogenic activities, we had to check each case to sort out typical episodes. In March and April, we found that there were several high biomass burning episodes based on the hourly CO emission rate: 26 through 28 March and 11 through 14 April. In the discussions below, we will focus on these specific episodes.

Figures 3 and 4 compare the regional distribution of the observed satellite parameters with the simulated results, including AOT and tropospheric nitrogen dioxide (NO_2). The model NO_2 column loading includes a total of 19 layers in CMAQ. The satellite NO_2 product used is Aura/OMI L3e tropospheric NO_2 at $0.25^{\circ} \times 0.25$ resolution, with cloudy pixels (cloud fraction >30%) screened out. The satellite observations on 28 March and 13 April were selected to evaluate the model performance. Gaps in satellite data are mainly due to possible cloud interference and limited satellite swath.

The satellite observation and model output demonstrate a similar spatial pattern. During both episodes, hot spots were observed and well simulated in the Southeast Asia region. There were two enhancement regions of NO_2, one in the Southeast Asia

ACPD
11, 3071–3115, 2011



region and the other in the industrialized eastern part of mainland China. Although the nitrogen oxides were not the main species emitted from biomass burning, high column concentrations of NO_2 were still present over most of Southeast Asia in both the remote sensing data and model simulation. The areas of high column NO_2 were confined to the source regions in Southeast and East Asia, (Fig. 3), suggesting negligible long-range transport of the relatively short-lived NO_2 and different sources of NO_2 in the two regions.

The high column loading of NO_2 in the northeastern part of China and the Pearl River Delta region was observed by various sensors (van der A et al., 2006) and was mainly due to the large consumption of fossil fuels by power plants, industries, and vehicles. AOD indicates the combination of all aerosol sources. The model-simulated AOD in the left panels was calculated based on the method used by Roy et al. (2007), which converts the aerosol dry mass concentration from the CMAQ model to AOD. As shown in Fig. 4, the model generally captured the observed magnitude and distribution of MODIS AOD on 28 March. The gaps in satellite AOD are mainly due to cloudy scenes and sun glint over the ocean.

Both satellite and CMAQ model show heavy aerosol loading over the biomass burning region in Southeast Asia and in the downwind areas, suggesting biomass burning activities and substantial long-range transport during the two episodes. Two high AOD regions were observed and simulated, one in Southeast Asia, which covered large areas extending eastward to the Western Pacific, and the other in a relatively small area located between 25° N and 30° N near the Yangtze River Region. On 13 April, the model seemed to predict lower AOD values in the northern part of China than the MODIS observation (Fig. 4). This underestimation was probably due to the lack of a dust module in CMAQ, as dust events derived from the Gobi desert in Northern China occurred during this period (Huang et al., 2010; Zhang et al., 2010).

As illustrated from the spatial distribution of NO_2 and AOD, the transport pathways of biomass burning plumes could be visualized. There were slightly different transport pathways between the two episodes. On March 28, aerosol originating from Southeast

ACPD
11, 3071–3115, 2011



Asia first circulated into the subtropical regions before migrating northward to the Central Pacific. Compared to aerosol, NO_2 transported over much shorter distances. The different transport patterns of these species were probably due to their different lifetimes; that is, NO_x ($NO + NO_2$) are highly reactive and quickly convert to other species such as depositions. On 13 April, the simulated plume clearly shifted to higher latitudes near the northeastern parts of China and even Japan, as illustrated by the AOD distribution. The main body of the outflows stayed around 15° N to 25° N, and there was an obvious concentration gradient along the transport pathway, although it was not evident in the first episode. In other words, the potential of biomass burning plumes to transport in the second episode was not as strong as in the first; neither was its impact on the downwind regions.

In summary, the model could relatively well simulate the spatial distribution of typical pollutants emitted from biomass burning. In the next section, we will not include the biomass burning emission of Southeast Asia in the model to quantitatively assess the regional influences caused by biomass burning.

4.3 Regional influences from biomass burning

In order to evaluate the impact of biomass burning on the source and the downstream regions, we performed a numerical experiment without the biomass burning emissions over Southeast Asia in the model to compare with the biomass burning emissions in the previous sections. Figures 5 and 6 illustrate the regional changes in CO, O_3, and $PM_{2.5}$ concentration with and without the biomass burning emissions during the two episodes (27 through 28 March and 13 through 14 April) in 2006. Note that the contours denote the perturbations between the base case and the case without biomass burning emissions in Southeast Asia. Red contoured lines denoted the percentage change of the species, which also represent the percentage contribution from biomass burning in Southeast Asia. The white arrows denote the wind vectors in the 15-th vertical layers at the altitude of 2.4 km. This layer was chosen mainly because of significant long-range transport above it, which would be discussed in the next section.

ACPD
11, 3071–3115, 2011



During the first episode on 27 March, the largest impact from the total biomass burning emissions covered areas of 10 to 25° N and 100 to 130° E, extending from Southeast Asia to the West Pacific. Corresponding to the satellite-observed spatial distribution in Figs. 3 and 4, the largest changes occurred over the source regions and over the transport pathways. The benefits from the scenario with the total biomass burning emissions were most prominent in Southeast Asia and nearby regions such as the Yunnan and Guangxi provinces in Southern China.

As illustrated in Fig. 5, without biomass burning in the source regions, concentrations of CO, O_3, and $PM_{2.5}$ were reduced by as much as 400 ppbv, 20 ppbv and 80 μg/m^3, respectively. The reduction percentages of the above three species were in the range of 10 to 60%, 10 to 20% and 30 to 70%, respectively. It seemed that the contribution percentage of O_3 from biomass burning was relatively small, in agreement with previous results (Zhang et al., 2003).

The downwind areas were also strongly influenced by the long-range transport of biomass burning plumes. On 27 March, the impact spread over the southeastern parts of mainland China, including the Pearl River Delta region and Fujian province. The impact from biomass burning on this region amounts to about 160 to 360 ppbv CO, 8 to 18 ppbv O_3 and 8 to 64 μg/m^3 $PM_{2.5}$. The biomass burning outflows may influence Taiwan and even the West Pacific. The transport impact could reach 20 to 50% on CO, 10 to 30% on O_3, and 70% on $PM_{2.5}$.

On 28 March, the biomass burning outflows transported more southward to the lower latitudes compared to the previous day, and the impact on the southeastern China was almost negligible (Fig. 5). The biomass burning plume was centered over the Western Pacific and the northern part of the Philippines; the magnitude of the biomass burning influence was similar to that on 27 March. The changes between days in these regions were likely related to the meteorological conditions. The northwesterly flow intensified on 28 March compared to the previous day, which pushed the plumes more southward. Moreover, the low-pressure system over Southern China moved over the South China Sea.

ACPD
11, 3071–3115, 2011



Along the major export pathway of the plumes, biomass burning derived CO and O_3 were spatially correlated with each other, probably indicating their common source. The transport pathways of biomass burning derived particles ($PM_{2.5}$) differed from CO and O_3, diffused quickly, and covered relatively short distances. On March 27, $PM_{2.5}$from biomass burning decreased from 40 to 80 μg/m^3 over the continent to 8 to 20 μg/m^3 over the ocean; thus, over 70% of the particles were scavenged during the transport. Compared to the gaseous pollutants, particles were more easily subject to scavenge through the wet/dry deposition.

As for the second episode on 13 and 14 April (Fig. 6), the impacts from biomass burning were not as widespread or intense. The effects of biomass burning centered over the source region areas of Southeast Asia, Southern China, and the regions between Southern China and the South China Sea. Beyond the Pearl River Delta region, the impact becomes less significant, although weak influence of transported plume may exist over oceanic areas as far as Japan (biomass burning derived CO and O_3 <100 ppbv and 6 ppbv, respectively with a negligible effect on $PM_{2.5}$).

Figure 7 shows the monthly average impact of biomass burning and wind patterns in March and April. In March, Southeast Asia biomass burning mainly affected southern parts of East Asia. Biomass burning contributed about 30 to 60%, 10 to 20%, and 20 to 70% of the total CO, O_3 and $PM_{2.5}$ concentrations, respectively. The long-range transport had a significant impact over the Yunnan and Guangxi provinces in China and over the South China Sea around Hainan Island, with 140 to 180 ppbv CO derived from biomass burning. The transported CO extended over broader areas such as the Fujian, Jiangxi, and Hunan provinces in China and the South China Sea. However, this effect was relatively insignificant, with less than 100 ppbv from biomass burning. As for O_3, the area influenced was broader than that of CO, with considerable biomass burning derived O_3 concentration of about 8 ppbv in the lower altitudes between 10° N and 15° N. There was also a belt over the West Pacific with a biomass burning derived O_3 concentration of 2 to 5 ppbv. The impact of biomass burning on $PM_{2.5}$ was mainly confined to the source areas of Southeast Asia.

ACPD
11, 3071–3115, 2011



There was a slight difference between the two months in that the impact from biomass burning reached the Yangtze River Delta region, as shown in Fig. 7. This difference is attributed to the change in wind patterns. In April, the easterly flows at the low latitudes turned to the southeasterly flows above 15° N, which could push the Southeast Asia outflows northward. The biomass burning impact on CO emissions remained in Southeast Asia and southern parts of China. The CO concentration that reached the Yangtze River Delta region was less than 60 ppbv, which contributed only a small percentage of the total concentration.

In April, ozone contributed by biomass burning plumes covered a region broader than that in March. Over most of the Pearl River Delta region, the Guangxi province, and large areas of South China Sea, the O_3 contribution by biomass burning plumes reached 9 to 11 ppbv. Additionally, the impact of biomass burning on the O_3 concentrations in parts of the Fujian, Jiangxi, and Hunan provinces reached about 8 ppbv, about 4 ppbv higher than in March. Another obvious difference was a high O_3 concentration belt extending from the East China Sea to the regions below Japan. The fast dispersion of $O_3$was probably related to the prevailing wind pattern during this period. As for $PM_{2.5}$, its transport was also more widespread and influenced major areas of southern China; the particulate contribution from biomass burning ranged from 10 to 30%.

4.4 Vertical distribution of biomass plumes

Figures 8 and 9 show the simulated altitude-longitude structure of CO, O_3, and $PM_{2.5}$ by biomass emission. Note that the contours denote the perturbations between the base case and the case without biomass burning emissions in Southeast Asia. Red contoured lines denote the percentage change of the species, which also represent the percentage contribution from biomass burning in Southeast Asia. The white arrows denote the wind vectors in the different vertical layers.

Two cross-sections at 15° N and 20° N were selected and compared, as this region was where the strongest biomass burning occurred. On 27 March at the cross section of 15° N, we found that there was strong zonal gradient in emissions. The blank areas

ACPD
11, 3071–3115, 2011



with negligible emissions were over the open oceans. High CO and O_3 emissions in the boundary layers around 100° E, 105–110° E, and 115–122° E were noted. At 100° E and 105–110° E, the concentration gradient was very small or had an increasing trend from surface to high altitudes, which indicated that the pollutants were emitted from the lands in the source region. Driven by the strong air convection in the tropics, the local emissions lofted to high altitudes and then transported. This is why a plume layer existed at high altitudes of about 2 to 8 km, which extended to around 130° E via the long range transport.

At around 115–122° E, an obvious decreasing gradient was observed from top to bottom, which suggests considerable deposition during the transport of biomass burning plumes. The percentage contributions of the transported plumes from biomass burning were 30 to 50% for CO, 20 to 40% for O_3 and over 70% for $PM_{2.5}$. The cross-section of 20° N was quite different from that of 15° N. The zonal gradient in emissions is smaller, as this cross-section covered more land. Pollutants started to deposit at around 112° E, as there was also a decreasing gradient at this longitude. The long-range transport contributed 60 to 70% to CO, 20 to 50% to O_3, and 80% to $PM_{2.5}$, respectively.

On 13 April, the transport of the biomass burning plumes was not as strong as on 27 March (Fig. 9), which is also consistent with our previous findings. On the cross-section of 15° N, the main body of pollutants was located between 98° E and 110° E. At the altitudes between 1km and 5km, there also existed a plume layer with a short tail that transported to around 120° E for CO and O_3. At the cross-section of 20° N, the biomass burning emission intensified. The subsidence of pollutants was found at 105-115° N, which was located at the junction of Vietnam and Guangxi province of China. The air pollutants could be depleted by various pathways during the subsidence.

As illustrated from the vertical structure of the biomass burning derived species, CO decreased from 400 ppbv at the top to about 160 to 200 ppv, with a depletion percentage of 50 to 60%. O_3 decreased from 20 ppbv to 8 to 10 ppbv, also with a depletion percentage of 50 to 60%, while $PM_{2.5}$ decreased from 80 μg/m^3 to 16~24 μg/m^3, with

ACPD
11, 3071–3115, 2011



a high depletion percentage of 70 to 80%. The high depletion percentage of particles during the subsidence probably was related with the interaction between particles and clouds. The contribution from biomass burning decreased with the decrease in altitude along the pathway of subsidence. As for CO, the contribution was about 50% from the top to about 30% at the bottom; for O_3, it was 60% to 20%; for $PM_{2.5}$, it was 60% to 20%. It seemed that the long-range transport of the biomass plumes exerted greater influence in the free troposphere than in the boundary layer.

5 Conclusions

In this paper, we evaluate the impact from Southeast Asia to East Asia during high biomass burning emissions periods. Through comparisons, we find that biomass burning plays a significant role in air quality in both local and downwind areas.

During the first episode on 27 March, the influence of biomass burning in the source region contributed to CO, O_3, and $PM_{2.5}$ concentrations as high as 400 ppbv, 20 ppbv, and 80 μg/m^3, respectively. The reduction percentages of the concentrations on the above three species without biomass burning were in the range of 10 to 60%, 10 to 20% and 30 to 70%, respectively. Also, the impacts due to long-range transport could spread over the southeastern parts of mainland China, including the Pearl River Delta region and the Fujian province in China. The impact from biomass burning on this region could contribute about 160 to 360 ppbv CO, 8 to 18 ppbv O_3 and 8 to 64 μg/m^3 $PM_{2.5}$, respectively; and the percentage impact could reach 20 to 50% on CO, 10 to 30% on O_3, and as high as 70% on $PM_{2.5}$. During the second episode period, the transport impact was a bit weaker to for the southern areas of China than the first episode period, probably reflecting differences in both biomass burning intensity and wind pattern. The impact for CO and O_3 can reached about 100 ppbv and 6 ppbv, respectively, while the impact on $PM_{2.5}$ was not very significant.

In March, biomass burning in Southeast Asia had significant impact on southern parts of East Asia, especially the Yunnan and Guangxi provinces in China and over the

ACPD
11, 3071–3115, 2011



South China Sea. Biomass burning contributed about 30 to 60%, 10 to 20%, and 20 to 70% to the total CO, O_3 and $PM_{2.5}$ concentrations, respectively. In April, due to slightly different wind patterns, CO effects could reach the Yangtze River Delta with an impact of about 60 ppbv (10 to 20%). High concentrations of O_3 extended farther in April. The O_3 concentration reduction ranged from 9 to 11 ppbv in the Pearl River Delta region, the Guangxi province in China, and large areas of the South China Sea. As for $PM_{2.5}$, its transport was also more widespread and influenced major areas of southern China, with the particulate contribution from biomass burning ranged from 10 to 30%.

Two cross-sections at 15° N and 20° N were selected to compare the vertical flux of biomass burning. In the source region (Southeast Asia), CO, O_3, and $PM_{2.5}$ concentrations had a strong upward tendency from surface to high altitudes. The transport became strong from 2 to 8 km in the free troposphere, and the pollutants were quickly transported eastward due to a strong western wind. The subsidence contributed 60 to 70% CO, 20 to 50% O_3, and 80% $PM_{2.5}$, respectively, to surface in the downwind area. Though NASA's BASE-ASIA conducted this biomass burning measurement, it might be less active in biomass burning in 2006. This modeling study might provide constraints of lower limit. An additional study is underway for an active biomass burning year to obtain an upper limit.

Supplementary material related to this article is available online at: http://www.atmos-chem-phys-discuss.net/11/3071/2011/acpd-11-3071-2011-supplement.pdf.

Acknowledgements. We thank Edward J. Hyer for providing FLAMBE biomass burning emission data. We thank NASA GSFC on funding support (grant no.: NNX09AG75G). Data products from SMART-COMMIT and Deep Blue groups of NASA GSFC are funded by the NASA Radiation Sciences Program, managed by Dr. Hal Maring. Lulin Mountain data was funded by the Taiwan National Science Council (96-2752-M-008-007-PAE) and Taiwan EPA (98-FA11-03-A015) managed by Neng-Huei Lin. Hong Kong data was obtained from Hong Kong Environmental Protection Department.

ACPD
11, 3071–3115, 2011



References

Air Sciences, Inc.: 2002 Fire Emission Inventory for the WRAP Region – Phase II, Prepared for the Western Governors Association/WRAP by Air Sciences, Inc., Denver, CO., 2005.

Allen, D. J., Kasibhatla, P., Thompson, A. M., Rood, R. B., Doddridge, B. G., Pickering, K. E., Hudson, R. D., and Lin, S. J.: Transport-induced interannual variability of carbon monoxide determined using a chemistry and transport model, J. Geophys. Res., 101(28), 28,655–628,669, 1996a.

Allen, D. J., Rood, R. B., Thompson, A. M., and Hudson, R. D.: Three-dimensional radon 222 calculations using assimilated meteorological data and a convective mixing algorithm, J. Geophys. Res., 101, 6871–6881, 1996b.

Alvarado, M. J. and Prinn, R. G.: Formation of ozone and growth of aerosols in young smoke plumes from biomass burning: 1. Lagrangian parcel studies, J. Geophys. Res., 114, D09306, doi:10.1029/2008JD011144, 2009.

Anderson, T. L., Covert, D. S., Marshall, S. F., Laucks, M. L., Charlson, R. J., Waggoner, A. P., Ogren, J. A., Caldow, R., Holm, R. L., Quant, F. R., Sem, G. J., Wiedensohler, A., Ahlquist, N. A., and Bates, T. S.: Performance characteristics of a high-sensitivity, three-wavelength, total scatter/backscatter nephelometer, J. Atmos. Ocean Tech., 13, 5, 967–986, 1996.

Anderson, T. L. and Ogren, J. A.: Determining aerosol radiative properties using the TSI 3563 integrating nephelometer, Aerosol Sci. Technol., 29, 1, 57–69, 1998.

Andreae, M. O. and Merlet, P.: Emission of trace gases and aerosols from biomass burning, Global Biogeochem. Cycles, 15, 4, 955–966, 2001.

Arnott, W. P., Hamasha, K., Moosmuller, H., Sheridan, P. J., and Ogren, J. A.: Towards aerosol light-absorption measurements with a 7-wavelength Aethalometer: Evaluation with a photoacoustic instrument and 3-wavelength nephelometer, Aerosol Sci. Technol., 39, 1, 17–29, 2005.

Byun, D. and Schere, K. L.: Review of the governing equations, computational algorithms, and other components of the models-3 Community Multiscale Air Quality (CMAQ) modeling system, Appl. Mech. Rev., 59(1–6), 51–77, 2006.

Byun, D. W. and Ching, J. K. S.: Science algorithm of the EPA Models-3 Community Multiscale Air Quality(CMAQ) Modeling System, EPA/600/R-699/030 pp, United States Environmental Protection Agency, Washington, DC, 1999.

Carmichael, G. R., Sakurai, T., Streets, D., Hozumi, Y., Ueda, H., Park, S. U., Fung, C., Han, Z.,

ACPD
11, 3071–3115, 2011



Kajino, M., Engardt, M., Bennet, C., Hayami, H., Sartelet, K., Holloway,T., Wang, Z., Kannari, A., Fu, J. S., Matsuda, K., Thongboonchoo, N., and Amann, M.: MICS-Asia II: The Model Intercomparison Study for Asia Phase II: Methodology and Overview of Findings, Atmos. Environ., 42, 3468–3490, 2008.

Chand, D., Guyon, P., Artaxo, P., Schmid, O., Frank, G. P., Rizzo, L. V., Mayol-Bracero, O. L., Gatti, L. V., and Andreae, M. O.: Optical and physical properties of aerosols in the boundary layer and free troposphere over the Amazon Basin during the biomass burning season, Atmos. Chem. Phys., 6, 2911–2925, doi:10.5194/acp-6-2911-2006, 2006.

Chang, D. and Song, Y.: Estimates of biomass burning emissions in tropical Asia based on satellite-derived data, Atmos. Chem. Phys., 10, 2335–2351, doi:10.5194/acp-10-2335-2010, 2010.

Choi, S. D. and Chang, Y. S.: Carbon monoxide monitoring in Northeast Asia using MOPITT: Effects of biomass burning and regional pollution in April 2000, Atmos. Environ., 40(4), 686–697, 2006.

Chuang, M. T., Fu, J. S., Jang, C. J., Chan, C. C., Ni, P. C., and Lee, C. T.: Simulation of A Long-range Transport Aerosols from the Asian Continent to Taiwan by a Southward Asian High-pressure System, Sci. Total. Environ., 406, 168–179, 2008.

Davidi, A., Koren, I., and Remer, L.: Direct measurements of the effect of biomass burning over the Amazon on the atmospheric temperature profile, Atmos. Chem. Phys., 9, 8211–8221, doi:10.5194/acp-9-8211-2009, 2009.

Deng, X. J., Tie, X. X., Zhou, X. J., Wo, D., Zhong, L. J., Tan, H. B., Li, F., Huang, X. Y., Bi, X. Y., and Deng, T.: Effects of Southeast Asia biomass burning on aerosols and ozone concentrations over the Pearl River Delta (PRD) region, Atmos. Environ., 42, 36, 8493–8501, 2008.

Dickerson, R. R. and Delany, A. C.: Modification of a commercial gas filter correlation CO detector for enhanced sensitivity, J. Atmos. Oceanic Technol., 5, 424–431, 1988.

Du, Y.: New Consolidation of Emission and Processing for Air Quality Modeling Assessment in Asia, Master Thesis, University of Tennessee, Knoxville, 2008.

Fast, J., Aiken, A. C., Allan, J., Alexander, L., Campos, T., Canagaratna, M. R., Chapman, E., DeCarlo, P. F., de Foy, B., Gaffney, J., de Gouw, J., Doran, J. C., Emmons, L., Hodzic, A., Herndon, S. C., Huey, G., Jayne, J. T., Jimenez, J. L., Kleinman, L., Kuster, W., Marley, N., Russell, L., Ochoa, C., Onasch, T. B., Pekour, M., Song, C., Ulbrich, I. M., Warneke, C., Welsh-Bon, D., Wiedinmyer, C., Worsnop, D. R., Yu, X.-Y., and Zaveri, R.: Evaluating

ACPD
11, 3071–3115, 2011



simulated primary anthropogenic and biomass burning organic aerosols during MILAGRO: implications for assessing treatments of secondary organic aerosols, Atmos. Chem. Phys., 9, 6191–6215, doi:10.5194/acp-9-6191-2009, 2009.

Freitas, S. R., Longo, K. M., and Andreae, M. O.: Impact of including the plume rise of vegetation fires in numerical simulations of associated atmospheric pollutants, Geophys. Res. Lett., 33, L17808, doi:10.1029/2006GL026608, 2006.

Fu, J. S., Jang, C. C., Streets, D. G., Li, Z., Kwok, R., Park, R., and Han, Z.: MICS-Asia II: Evaluating Gaseous Pollutants in East Asia Using An Advanced Modeling System: Models-3/CMAQ System, Atmos. Environ., 42, 3571–3583, 2008.

Fu, J. S., Yeh, F. L., Carey, C. J., Chen, R. J. and Chuang, M. T.: Air Quality Modelling – An Investigation of The Merits of CMAQ In The Analysis of Trans-boundary Air Pollution From Continents to Small Islands, Int. J. Environ. Tech. Manag., 10, 22–31, 2009a.

Fu, J. S., Streets, D. G., Jang, C. J., Hao, J., He, K., Wang, L., Zhang, Q. Modeling Regional/Urban Ozone and Particulate Matter in Beijing, China, J. Air Waste Manag., 59, 37–44, 2009b.

Gustafsson, O., Krusa, M., Zencak, Z., Sheesley, R. J., Granat, L., Engstrom, E., Praveen, P. S., Rao, P. S. P., Leck, C., and Rodhe, H.: Brown Clouds over South Asia: Biomass or Fossil Fuel Combustion?, Science, 323, 5913, 495–498, 2009.

Guyon, P., Frank, G. P., Welling, M., Chand, D., Artaxo, P., Rizzo, L., Nishioka, G., Kolle, O., Fritsch, H., Silva Dias, M. A. F, Gatti, L. V., Cordova, A. M., and Andreae, M. O.: Airborne measurements of trace gas and aerosol particle emissions from biomass burning in Amazonia, Atmos. Chem. Phys., 5, 2989–3002, doi:10.5194/acp-5-2989-2005, 2005.

Haywood, J. M., Pelon, J., Formenti, P., Bharmal, N., Brooks, M., Capes, G., Chazette, P., Chou, C., Christopher, S., Coe, H., Cuesta, J., Derimian, Y., Desboeufs, K., Greed, G., Harrison, M., Heese, B., Highwood, E. J., Johnson, B., Mallet, M., Marticorena, B., Marsham, J., Milton, S., Myhre, G., Osborne, S. R., Parker, D. J., Rajot, J. L., Schulz, M., Slingo, A., Tanre, D., and Tulet, P.: Overview of the Dust and Biomass-burning Experiment and African Monsoon Multidisciplinary Analysis Special Observing Period-0, J. Geophys. Res., 113, D00C17, doi:10.1029/2008JD010077, 2008.

Heald, C. L., Jacob, D. J., Fiore, A. M., Emmons, L. K., Gille, J. C., Deeter, M. N., Warner, J., Edwards, D. P., Crawford, J. H., Hamlin, A. J., Sachse, G. W., Browell, E. V., Avery, M. A., Vay, S. A., Westberg, D. J., Blake, D. R., Singh, H. B., Sandholm, S. T., Talbot, R. W., and Fuelberg, H. E.: Asian outflow and trans-Pacific transport of carbon monoxide and

ACPD
11, 3071–3115, 2011



ozone pollution: An integrated satellite, aircraft, and model perspective, J. Geophys. Res., 108(D24), doi:10.1029/2003JD003507, 4804, 2003.
Hertel, O., Berkowicz, R., Christensen, J., and Hov, O.: Test of two numerical schemes for use in atmospheric transport-chemistry models, Atmos. Environ., 27A, 2591–2611, 1993.
Hsu, N. C., Tsay, S.-C., King, M. D., and Herman, J. R.: Aerosol properties over bright-reflecting source regions, IEEE Trans. Geosci. Remote Sens., 42, 557–569, 2004.
Hsu, N. C., Tsay, S.-C., King, M. D., and Herman, J. R.: Deep blue retrievals of Asian aerosol properties during ACE-Asia, IEEE Trans. Geosci. Remote Sens., 44, 3180–3195, 2006.
Huang, K., Zhuang, G., Lin, Y., Li, J., Sun, Y., Zhang, W., and Fu, J. S.: Relation between optical and chemical properties of dust aerosol over Beijing, China, J. Geophys. Res., 115, D00K16, doi:10.1029/2009JD013212, 2010.
Hyer, E. J., Allen, D. J., and Kasischke, E. S.: Examining injection properties of boreal forest fires using surface and satellite measurements of CO transport, J. Geophys. Res., 112, D18307, doi:10.1029/2006JD008232, 2007.
IPCC: The Physical Science Basis. Contribution of Working Group I to the Fourth Assessment Report of the Intergovernmental Panel on Climate Change, edited by: Solomon, S., Qin, D., Manning, M., Chen, Z., Marquis, M., Averyt, K. B., Tignor, M., and Miller, H. L., Cambridge University Press, Cambridge, United Kingdom and New York, NY, USA, 2007.
Kaufman, Y., Tanàe, D., Remer, L., Vermote, E., Chu, A., and Holben, B.: Operational remote sensing of tropospheric aerosol over land from EOS moderate resolution imaging spectroradiometer, J. Geophys. Res., 102(D14), 17051–17067, 1997.
Kim, J., Yoon, S. C., Jefferson, A., and Kim, S. W.: Aerosol hygroscopic properties during Asian dust, pollution, and biomass burning episodes at Gosan, Korea in April 2001, Atmos. Environ., 40, 8, 1550–1560, 2006.
Kim, S.-W., Chazette, P., Dulac, F., Sanak, J., Johnson, B., and Yoon, S.-C.: Vertical structure of aerosols and water vapor over West Africa during the African monsoon dry season, Atmos. Chem. Phys., 9, 8017–8038, doi:10.5194/acp-9-8017-2009, 2009.
Krotkov, N. A., McClure, B., Dickerson, R. R., Carn, S. A., Li, C., Bhartia, P. K., Yang, K., Krueger, A. J., Li, Z. Q., Levelt, P. F., Chen, H. B., Wang, P. C., and Lu, D. R.: Validation of SO2 retrievals from the Ozone Monitoring Instrument over NE China, J. Geophys. Res., 113, D16S40, doi:10.1029/2007JD008818, 2008.
Leung, F.-Y. T., Logan, J. A., Park, R., Hyer, E. J., Kasischke, E. S., Streets, D. G., and Yurganov, L.: Impacts of enhanced biomass burning in the boreal forests in 1998 on tropospheric

ACPD
11, 3071–3115, 2011



chemistry and the sensitivity of model results to the injection height of emissions, J. Geophys. Res., 112, D10313, doi:10.1029/2006JD008132, 2007.
Levelt, P. F., van den Oord, G. H. J., Dobber, M. R., Malkki,Huib Visser Johan de Vries, A., Stammes, P., Lundell, J. O. V., and Saari, H.: The Ozone Monitoring Instrument, Ieee Transactions on Geoscience and Remote Sensing, 44, 5, 1093–1101, 2006.
Levy, R. C., Remer, L. A., Mattoo, S., Vermote, E., and Kaufman, Y. J.: Second-generation algorithm for retrieving aerosol properties over land from MODIS spectral reflectance, J. Geophys. Res., 112, D13211, doi:10.1029/2006JD007811, 2007.
Li, C., Krotkov, N. A., Dickerson, R. R., Li, Z. Q., Yang, K., and Chin, M.: Transport and evolution of a pollution plume from northern China: A satellite-based case study, J. Geophys. Res., 115, D00K03, doi:10.1029/2009JD012245, 2010a.
Li, C., Tsay, S. C., Fu, J. S., Dickerson, R., Ji, Q., Bell, S., Gao, Y., Zhang, W., Huang, J., Li, Z., and Chen, H.: Anthropogenic Air Pollution Observed near Dust Source Regions in Northwestern China during Springtime 2008, J. Geophys. Res., D00K22, doi:10.1029/2009JD013659, 2010b.
Li, C., Zhang, Q., Krotkov, N. A., Streets, D. G., He, K. B., Tsay, S. C., and Gleason, J. F.: Recent large reduction in sulfur dioxide emissions from Chinese power plants observed by the Ozone Monitoring Instrument, Geophys. Res. Lett., 37, L08807, doi:10.1029/2010GL042594, 2010c.
Lin, C.-Y., Hsu, H.-m., Lee, Y. H., Kuo, C. H., Sheng, Y.-F., and Chu, D. A.: A new transport mechanism of biomass burning from Indochina as identified by modeling studies, Atmos. Chem. Phys., 9, 7901–7911, doi:10.5194/acp-9-7901-2009, 2009.
Liu, H. Y., Chang, W. L., Oltmans, S. J., Chan, L. Y., and Harris, J. M.: On springtime high ozone events in the lower troposphere from Southeast Asian biomass burning, Atmos. Environ., 33(15), 2403–2410, 1999.
Luke, W. T.: Evaluation of a commercial pulsed fluorescence detector for the measurement of low-level SO_2 concentrations during the gas-phase sulfur intercomparison experiment, J. Geophys. Res., 102(D13), 16255–16265, 1997.
Mari, C. H., Cailley, G., Corre, L., Saunois, M., Attié, J. L., Thouret, V., and Stohl, A.: Tracing biomass burning plumes from the Southern Hemisphere during the AMMA 2006 wet season experiment, Atmos. Chem. Phys., 8, 3951–3961, doi:10.5194/acp-8-3951-2008, 2008.
Martin, R. V.: Satellite remote sensing of surface air quality, Atmos. Environ., 42(34), 7823–7843, 2008.

ACPD
11, 3071–3115, 2011



Martins, J. A., Dias, M. A. F. S., and Goncalves, F. L. T.: Impact of biomass burning aerosols on precipitation in the Amazon: A modeling case study, J. Geophys. Res., 114, D02207, doi:10.1029/2007JD009587, 2009.
Milton, S. F., Greed, G., Brooks, M. E., Haywood, J., Johnson, B., Allan, R. P., Slingo, A., and Grey, W. M. F.: Modeled and observed atmospheric radiation balance during the West African dry season: Role of mineral dust, biomass burning aerosol, and surface albedo, J. Geophys. Res., 113, D00C02, doi:10.1029/2007JD009741, 2008.
Moraes, E. C., Franchito, S. H., and Rao, V. B.: Effects of biomass burning in Amazonia on climate: A numerical experiment with a statistical-dynamical model, J. Geophys. Res., 109(D5), D05109, doi:10.1029/2003JD003800, 2004.
Morris, R.: Application of Multiple Models to Simulation Fine Particulate in the Southeastern US, National RPO Modeling Meeting, Denver, CO., 2005.
Morris, R. E., Koo, B., Guenther, A., Yarwood, G., McNally, D., Tesche, T. W., Tonnesen, G., Boylan, J., and Brewer, P.: Model sensitivity evaluation for organic carbon using two multi-pollutant air quality models that simulate regional haze in the southeastern United States, Atmos. Environ., 40(26), 4960–4972, 2006.
Myhre, G., Hoyle, C. R., Berglen, T. F., Johnson, B. T., and Haywood, J. M.: Modeling of the solar radiative impact of biomass burning aerosols during the Dust and Biomass-burning Experiment (DABEX), J. Geophys. Res., 113, D00C16, doi:10.1029/2008JD009857, 2008.
Nam, J., Wang, Y., Luo, C., and Chu, D. A.: Trans-Pacific transport of Asian dust and CO: accumulation of biomass burning CO in the subtropics and dipole structure of transport, Atmos. Chem. Phys., 10, 3297–3308, doi:10.5194/acp-10-3297-2010, 2010.
Patra, P. K., Ishizawa, M., Maksyutov, S., Nakazawa, T., and Inoue, G.: Role of biomass burning and climate anomalies for land-atmosphere carbon fluxes based on inverse modeling of atmospheric CO_2, Global Biogeochem. Cycles, 19(3), GB3005, doi:10.1029/2004GB002258, 2005.
Potter, C., Genovese, V. B., Klooster, S., Bobo, M., and Torregrosa, A.: Biomass burning losses of carbon estimated from ecosystem modeling and satellite data analysis for the Brazilian Amazon region, Atmos. Environ., 35(10), 1773–1781, 2001.
Pouliot, G.: A Tale of Two Models: A Comparison of the Biogenic Emission Inventory System (BEIS3.14) and Model of Emissions of Gases and Aerosols from Nature (MEGAN 2.04), paper presented at 7th Annual CMAS Conference, Chapel Hill, NC, 7 October 2008, 2008.
Pouliot, G. and Pierce, T. E.: Integration of the Model of Emissions of Gases and Aerosols from

ACPD
11, 3071–3115, 2011



Nature (MEGAN) into the CMAQ Modeling System, paper presented at 18th International Emission Inventory Conference, Baltimore, Maryland, 14–17 April 2009, 2009.
Reid, J. S., Hyer, E. J., Prins, E. M., Westphal, D. L., Jianglong, Z., Jun, W., Christopher, S. A., Curtis, C. A., Schmidt, C. C., Eleuterio, D. P., Richardson, K. A., and Hoffman, J. P.: Global Monitoring and Forecasting of Biomass-Burning Smoke: Description of and Lessons From the Fire Locating and Modeling of Burning Emissions (FLAMBE) Program, Selected Topics in Applied Earth Observations and Remote Sensing, IEEE Selected Topics in Applied Earth Observations and Remote Sensing, 2(3), 144–162, 2009.
Reid, J. S., Koppmann, R., Eck, T. F., and Eleuterio, D. P.: A review of biomass burning emissions part II: intensive physical properties of biomass burning particles, Atmos. Chem. Phys., 5, 799–825, doi:10.5194/acp-5-799-2005, 2005.
Remer, L. A., Kaufman Y. J., Tanre, D., Mattoo, S., Chu, D. A., Martins, J. V., Li, R. R., Ichoku, C., Levy, R. C., Kleidman, R. G., Eck, T. F., Vermote, E., and Holben, B. N.: The MODIS aerosol algorithm, products, and validation, J. Atmos. Sci., 62(4), 947–973, 2005.
Richter, A., Burrows, J. P., Nuss, H., Granier, C., and Niemeier, U.: Increase in tropospheric nitrogen dioxide over China observed from space, Nature, 437(7055), 129–132, 2005.
Rissler, J., Vestin, A., Swietlicki, E., Fisch, G., Zhou, J., Artaxo, P., and Andreae, M. O.: Size distribution and hygroscopic properties of aerosol particles from dry-season biomass burning in Amazonia, Atmos. Chem. Phys., 6, 471–491, doi:10.5194/acp-6-471-2006, 2006.
Roy, B., Mathur, R., Gilliland, A. B., and Howard, S. C.: A comparison of CMAQ-based aerosol properties with IMPROVE, MODIS, and AERONET data, J. Geophys. Res., 112, D14301, doi:10.1029/2006JD008085, 2007.
Sherwood, S.: A microphysical connection among biomass burning, cumulus clouds, and stratospheric moisture, Science, 295(5558), 1272–1275, 2002.
Sheu, G. R., Lin, N. H., Wang, J. L., Lee, C. T., Yang, C. F. O., and Wang, S. H. : Temporal distribution and potential sources of atmospheric mercury measured at a high-elevation background station in Taiwan, Atmos. Environ., 44(20), 2393–2400, 2010.
Sinha, P., L. Jaegle, Hobbs, P. V., and Liang, Q.: Transport of biomass burning emissions from southern Africa, J. Geophys. Res., 109(D20), D20204,, doi:10.1029/2004JD005044, 2004.
Staudt, A. C., Jacob, D. J., Logan, J. A., Bachiochi, D., Krishnamurti, T. N., and Poisson, N.: Global chemical model analysis of biomass burning and lightning influences over the South Pacific in austral spring, J. Geophys. Res., 107(D14), 4200, doi:10.1029/2000JD000296, 2002.

ACPD
11, 3071–3115, 2011



Streets, D. G., Bond, T. C., Lee, T., and Jang, C.: On the future of carbonaceous aerosol emissions, J. Geophys. Res., 109(D24), D24212, doi:10.1029/2004JD004902, 2004.
Streets, D. G., Fu, J. S., Jang, C., Hao, J., He, K., Tang, X., Zhang, Y., Li, Z., Zhang, Q., Wang, L., Wang, B., and Yu, C.: Air quality during the 2008 Beijing Olympic games, Atmos. Environ., 41(3), 480–492, 2007.
Swap, R. J., Annegarn, H. J., Suttles, J. T., King, M. D., Platnick, S., Privette, J. L., and Scholes, R. J.: Africa burning: A thematic analysis of the Southern African Regional Science Initiative (SAFARI 2000), J. Geophys. Res., 108(D13), doi:10.1029/2003JD003747, 8465, 2003.
Tang, Y. H., Carmichael, G. R., Woo, J. H., Thongboonchoo, N., Kurata, G., Uno, I., Streets, D. G., Blake, D. R., Weber, R. J., Talbot, R. W., Kondo, Y., Singh, H. B., and Wang, T.: Influences of biomass burning during the Transport and Chemical Evolution Over the Pacific (TRACE-P) experiment identified by the regional chemical transport model, J. Geophys. Res., 108(D21), 8824, doi:10.1029/2002JD003110, 2003.
Tanàe, D., Kaufman, Y. J., Herman, M., and Mattoo, S.: Remote sensing of aerosol properties over oceans using the MODIS/EOS spectral radiances, J. Geophys. Res., 102(D14), 16971–16988, 1997.
Tesche, T. W., Morris, R., Tonnesen, G., McNally, D., Boylan, J., and Brewer, P.: CMAQ/CAMx annual 2002 performance evaluation over the eastern US, Atmos. Environ., 40(26), 4906–4919, 2006.
Thompson, A. M., Witte, J. C., Hudson, R. D., Guo, H., Herman, J. R., and Fujiwara, M.: Tropical Tropospheric Ozone and Biomass Burning, Science, 291(5511), 2128–2132, 2001.
Trentmann, J., Andreae, M. O., Graf, H. F., Hobbs, P. V., Ottmar, R. D., and Trautmann, T.: Simulation of a biomass-burning plume: Comparison of model results with observations, J. Geophys. Res., 107(D1–D2), 4013, doi:10.1029/2001JD000410, 2002.
USEPA: Guidance on the Use of Models and Other Analyses for Demonstrating Attainment of Air Quality Goals for Ozone, $PM_{2.5}$ and Regional Haze, EPA-454/B-07e002, USEPA, 2007.
van der A, R. J., Peters, D. H. M. U., Eskes, H., Boersma, K. F., Van Roozendael, M., De Smedt, I., and Kelder, H. M.: Detection of the trend and seasonal variation in tropospheric NO_2 over China, J. Geophys. Res., 111, D12317, doi:10.1029/2005JD006594, 2006.
van der Werf, G. R., Randerson, J. T., Giglio, L., Collatz, G. J., Kasibhatla, P. S., and Arellano Jr., A. F.: Interannual variability in global biomass burning emissions from 1997 to 2004, Atmos. Chem. Phys., 6, 3423–3441, doi:10.5194/acp-6-3423-2006, 2006.
Walcek, C. J. and Aleksic, N. M.: A Simple but Accurate Mass Conservative Peak-Preserving,

ACPD
11, 3071–3115, 2011



Mixing Ratio Bounded Advection Algorithm with Fortran Code, Atmos. Environ., 32, 3863–3880, 1998.
Wang, L., Hao, J., He, K., Wang, S., Li, J., Zhang, Q., Streets, J. S., Fu, C. J., Jang, H., Takekawa, H., and Chatani, S.: Modeling Study on PM10 Pollution in Beijing: Regional Contributions and Control Implications, J. Air Waste Manag., 58, 1057–1069, 2008.
Wang, L., Carey, J., Zhang, Y., Wang, K., Zhang, Q., Streets, D., Fu, J., Lei, Y., Schreifels, J., He, K., Hao, J., Lam, Y. F., Lin, J., Meskhidze, N., Voorhees, S., Evarts, D., and Phillips, S.: Assessment of air quality bene?ts from national air pollution control policies in China. Part I: Background, emission scenarios and evaluation of meteorological predictions, Atmos. Environ., 44, 3442–3448, 2010a.
Wang, L., Carey, J., Zhang, Y., Wang, K., Zhang, Q., Streets, D., Fu, J., Lei, Y., Schreifels, J., He, K., Hao, J., Lam, Y. F., Lin, J., Meskhidze, N., Voorhees, S., Evarts, D., Phillips, S.: Assessment of air quality benefits from national air pollution control policies in China, Part II: Evaluation of air quality predictions and air quality benefits assessment, Atmos. Environ., 44, 3449–3457. 2010b.
Wang, S. H., Lin, N. H., Chou, M. D., and Woo, J. H.: Estimate of radiative forcing of Asian biomass-burning aerosols during the period of TRACE-P, J. Geophys. Res., 112(D10), D10222, doi:10.1029/2006JD007564, 2007.
Wesely, M. L.: Parameterization of Surface Resistances to Gaseous Dry Deposition in Regional-Scale Numerical-Models, Atmos. Environ., 23, 1293–1304, 1989.
Winkler, H., Formenti, P., Esterhuyse, D. J., Swap, R. J., Helas, G., Annegarn, H. J., and Andreae, M. O.: Evidence for large-scale transport of biomass burning aerosols from sun-photometry at a remote South African site, Atmos. Environ., 42(22), 5569–5578, 2008.
Xu, J., Zhang, Y., Fu, J. S., and Wang, W.: Process Analysis of Typical Ozone Episode in Summer over Beijing Area, Sci. Total Environ., 399, 147–157, 2008.
Zhang, M. G., Uno, I., Carmichael, G. R., Akimoto, H., Wang, Z. F., Tang, Y. H., Woo, J. H., Streets, D. G., Sachse, G. W., Avery, M. A., Weber R. J., and Talbot, R. W.: Large-scale structure of trace gas and aerosol distributions over the western Pacific Ocean during the Transport and Chemical Evolution Over the Pacific (TRACE-P) experiment, J. Geophys. Res., 108(D21), 8820, doi:10.1029/2002JD002946, 2003.
Zhang, Q., Streets, D. G., Carmichael, G. R., He, K. B., Huo, H., Kannari, A., Klimont, Z., Park, I. S., Reddy, S., Fu, J. S., Chen, D., Duan, L., Lei, Y., Wang, L. T., and Yao, Z. L.: Asian emissions in 2006 for the NASA INTEX-B mission, Atmos. Chem. Phys., 9, 5131–5153,

ACPD
11, 3071–3115, 2011



doi:10.5194/acp-9-5131-2009, 2009.
Zhang, W., Zhuang, G., Huang, K., Li, J., Zhang, R., Wang, Q., Sun, Y., Fu, J. S., Chen, Y., Xu, D., and Wang, W.: Mixing and transformation of Asian dust with pollution in the two dust storms over the northern China in 2006, Atmos. Environ., 44(28), 3394–3403, 2010.
Zhang, Y., Fu, R., Yu, H. B., Dickinson, R. E., Juarez, R. N., Chin, M. A., and Wang, H.: A regional climate model study of how biomass burning aerosol impacts land-atmosphere interactions over the Amazon, J. Geophys. Res., 113(D14), D14S15, doi:10.1029/2007JD009449, 2008.

ACPD
11, 3071–3115, 2011



Table 1. Model configuration of CMAQ.

Chemistry model	CMAQ 4.6
Horizontal resolution	27 km × 27 km
Vertical resolution	19 sigma-pressure levels (with the top pressure of 100 mb)
Projection	Lambert Conformal Conic
Advection	piecewise parabolic scheme
Vertical diffusion	K-theory
Gas-phase chemistry	CB05 with Euler Backward Iterative (EBI) (Hertel et al., 1993) solver
Dry deposition	Wesely[Wesely (1989)]
Wet deposition	Henry's law
Aqueous chemistry	Walcek[Walcek and Aleksic (1998)]
Aerosol mechanism	AE4

ACPD
11, 3071–3115, 2011



Table 2. Model configuration of WRF.

Meteorology model	WRF V3.1.1
Explicit precipitation scheme	WRF single-moment 3-class scheme
Longwave Radiation	RRTM
Shortwave Radiation	Dudhia scheme
Surface-layer option	MM5 similarity (Monin-Obukhov scheme)
Land-surface	Thermal diffusion scheme
advection	global mass-conserving scheme
planetary boundary layer(PBL) scheme:	YSU
Cumulus option	Grell

ACPD
11, 3071–3115, 2011



Table 3. Southeast Asia carbon emissions from GFEDv2 and FLAMBE.

	GFEDv2_carbon (Tg/mon)	FLAMBE_carbon (Tg/mon)	FLAMBE/ GFEDv2
Jan	5.54	14.01	2.53
Feb	8.06	35.79	4.44
Mar	28.00	220.90	7.89
Apr	13.43	156.22	11.63
May	0.90	8.74	9.70
Jun	0.21	1.39	6.72
Jul	0.03	0.12	3.81
Aug	0.02	0.08	3.54
Sep	0.10	0.23	2.30
Oct	0.12	0.47	4.02
Nov	0.55	1.92	3.47
Dec	2.08	7.60	3.66
Annual (Tg/year)	59.04	447.47	7.58

ACPD
11, 3071–3115, 2011



Table 4. Outside Southeast Asia in the domain (Referred as East Asia) carbon emissions from GFEDv2 and FLAMBE.

Month	GFEDv2_carbon_emis (Tg/mon)	FLAMBE_carbon_emis (Tg/mon)	FLAMBE/GFEDv2
Jan	0.40	4.97	12.39
Feb	1.16	10.13	8.73
Mar	18.24	84.79	4.65
Apr	1.58	21.13	13.39
May	1.78	6.08	3.42
Jun	1.24	1.25	1.01
Jul	0.94	0.66	0.70
Aug	1.36	1.09	0.80
Sep	0.44	0.92	2.09
Oct	0.73	2.21	3.02
Nov	0.59	3.31	5.65
Dec	0.33	3.27	9.97
sum (Tg/year)	28.79	139.81	4.86

ACPD
11, 3071–3115, 2011



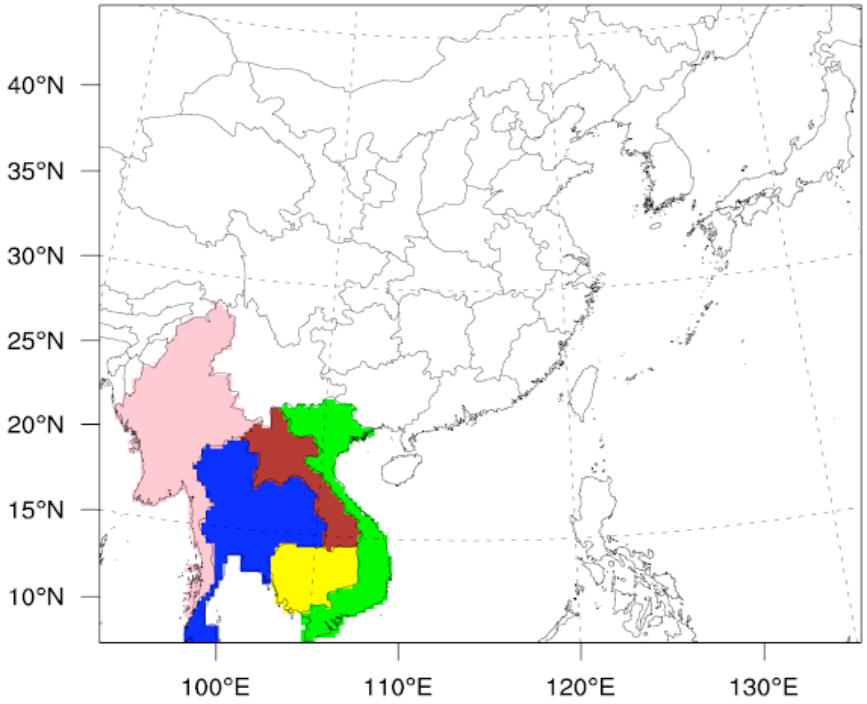


Fig. 1. Fiver biomass burning countries in Southeast Asia in this study with different colors representing the countries (Pink: Burma; Bule: Thailand; Yellow: Cambodia; Red: Laos; Green: Vietnam).

ACPD
11, 3071–3115, 2011



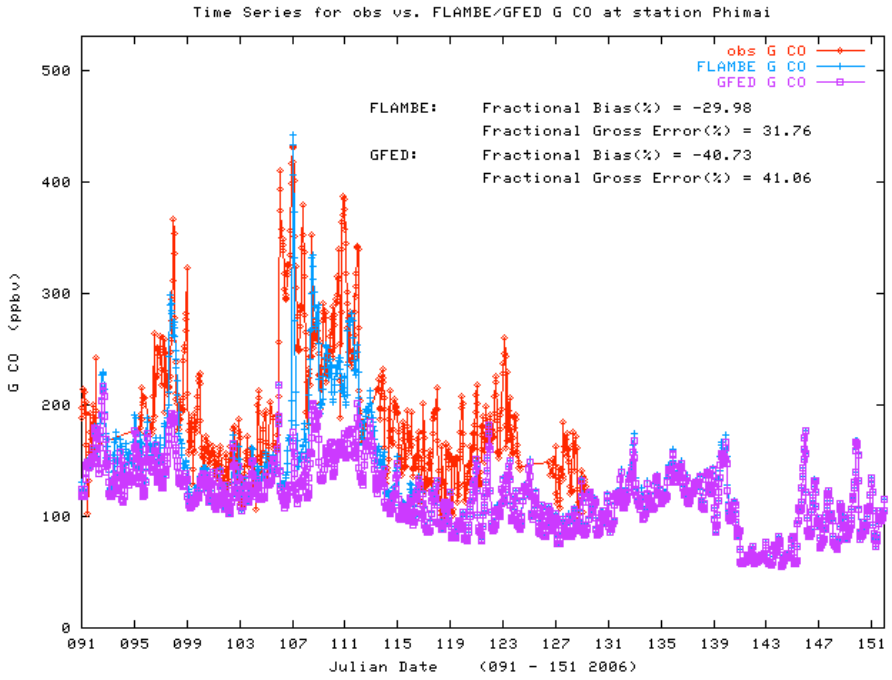


Fig. 2. Model Performance of Phimai between FLAMBE and GFED biomass burning emissions.

ACPD
11, 3071–3115, 2011



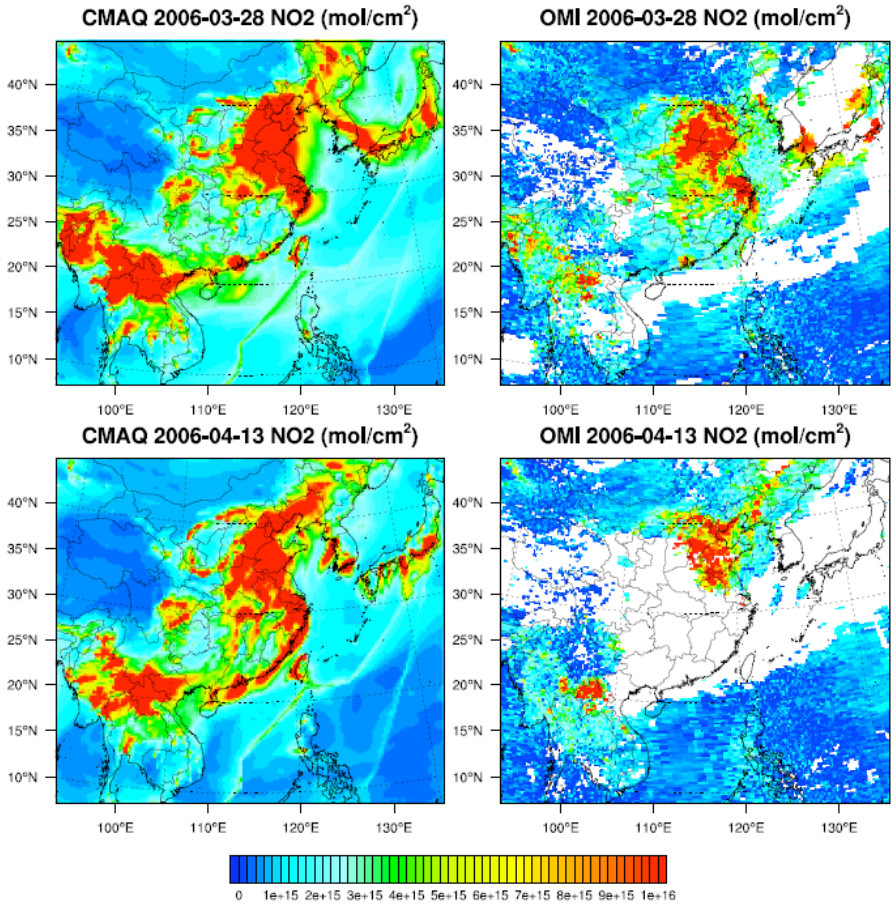


Fig. 3. Comparison between (left) model simulated and (right) satellite-retrieved tropospheric NO_2 column amounts on (top) 28 March and (bottom) 13 April 2006.

ACPD
11, 3071–3115, 2011



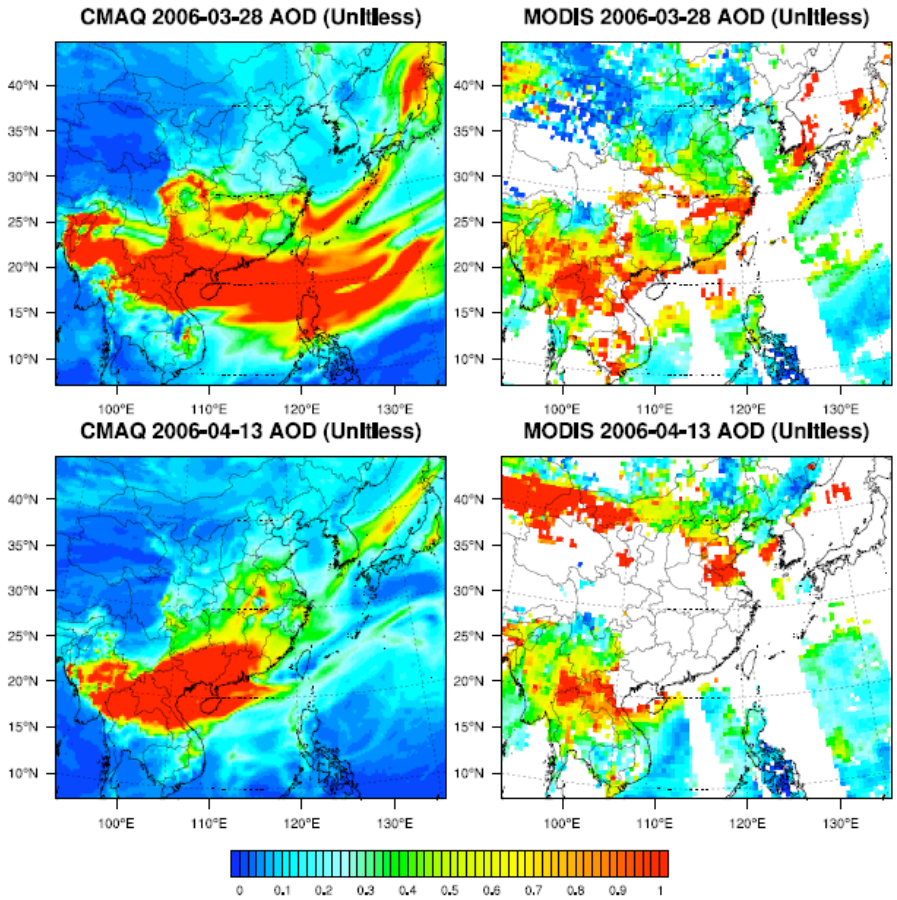


Fig. 4. Comparison between (left) model simulated and (right) satellite-retrieved aerosol optical depth (AOD). Panels on the right show the composite Aqua/MODIS C005 Deep Blue and dark-target AOD at 550 nm, gridded to 0.5°×0.5° resolution.

ACPD
11, 3071–3115, 2011



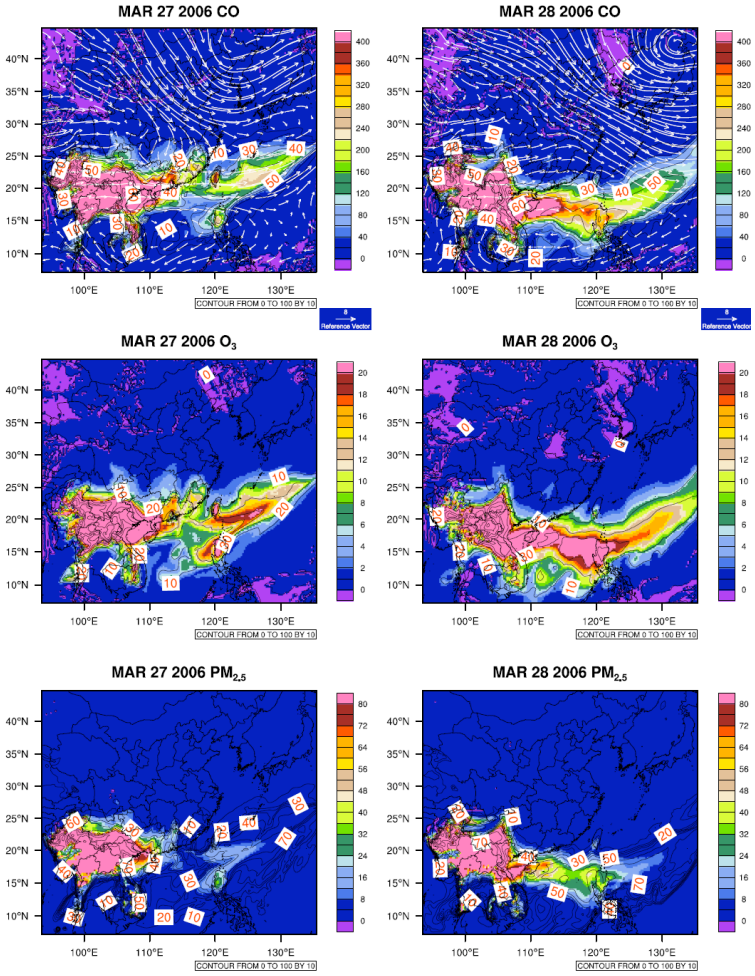


Fig. 5. Impact of biomass burning in Southeast Asia during episode days 27–28 March 2006.

ACPD
11, 3071–3115, 2011



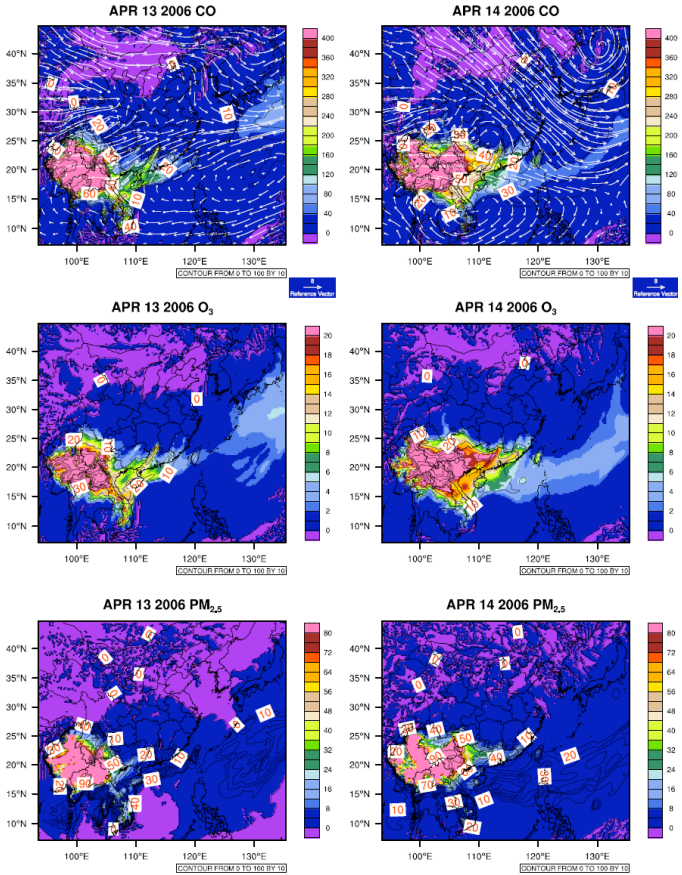


Fig. 6. Impact of biomass burning in Southeast Asia during episode days 13–14 April 2006.

ACPD
11, 3071–3115, 2011



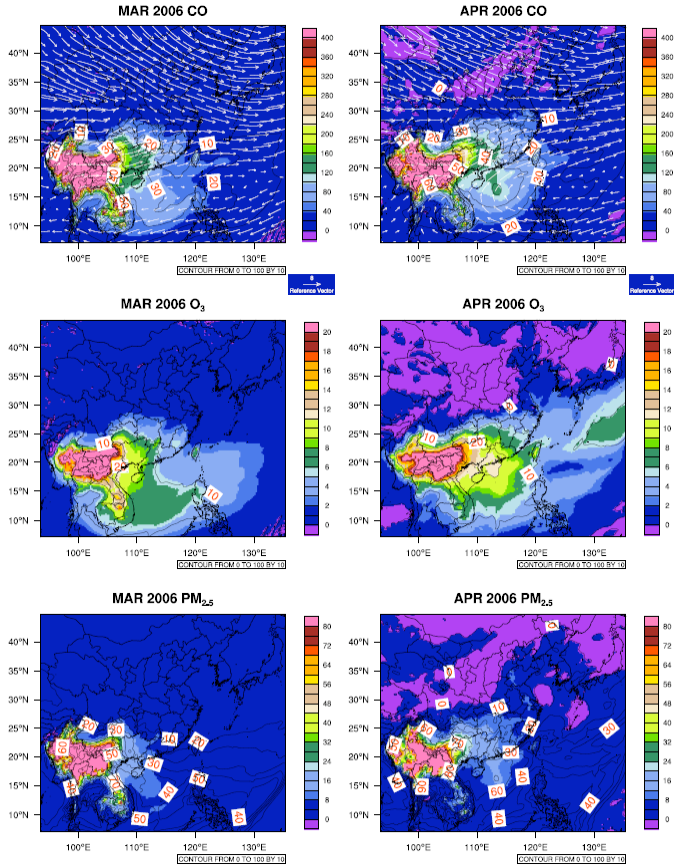


Fig. 7. Month average impact of biomass burning in Southeast Asia during in March and April 2006.

ACPD
11, 3071–3115, 2011



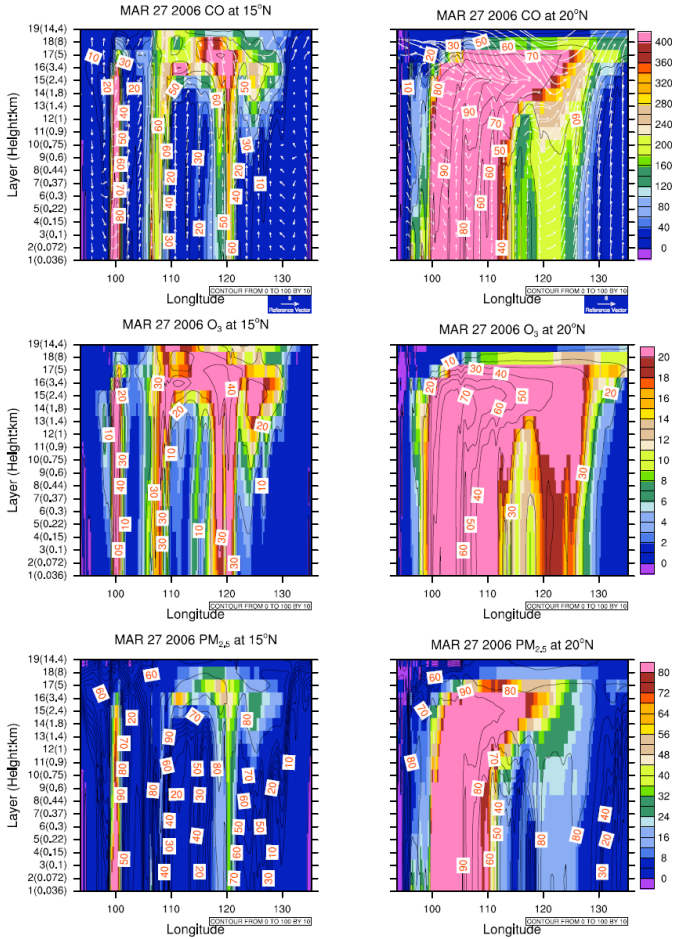


Fig. 8. Cross section of biomass burning in Southeast Asia during episode days on 27–28 March 2006.

ACPD
11, 3071–3115, 2011



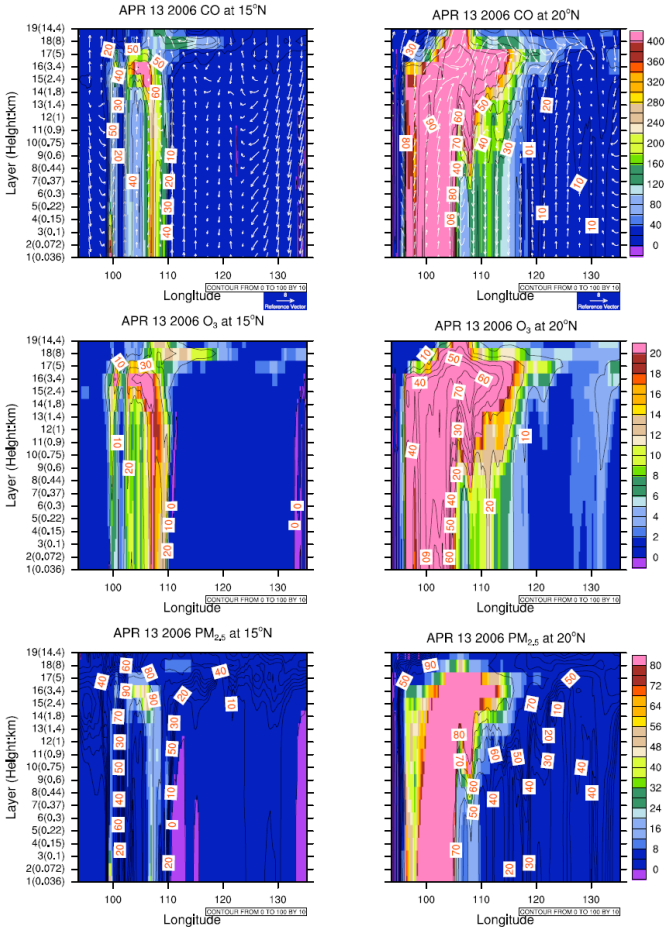


Fig. 9. Same as Fig. 8 but for the episode days during 13–14 April 2006.

ACPD
11, 3071–3115, 2011

